Electronic Supplementary Material (ESI) for Physical Chemistry Chemical Physics.

Supporting Information

(1) Sequential correlation of the photon stream

To study the influence of the water content, which did not exceed on average 10 Vol-% and below, on the $g^{(2)}$ decay, the fluorescence signal of (**2**) at 2 mM tfa concentration is analyzed in more detail. The photon stream, which was recorded over 4 hours, is equally split and is correlated for each of the four hours of measurement time. The separate correlations of each hour of measurement time do not yield significant deviations from each other with respect to the decay constants within the error margin of the experiment. We conclude that the behavior of H^+ in dmso is not significantly altered up to a water content of 10 Vol-%.

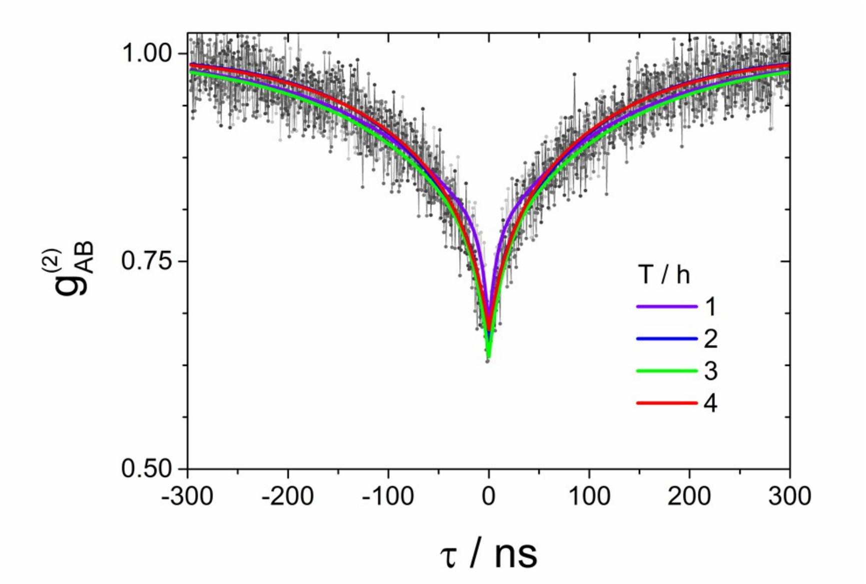

Fig. S1: Experimental correlation function of (**2**) at 2 mM tfa concentration. Each full hour of the photon stream, which was recorded over 4 hours, is correlated separately. The same result is obtained in other runs, where one-hour cut-outs could be studied.

Tab. 1: Fit parameters of $g_{AB}^{(2)}$. t_l: long-time component, t_s: short-time component. The dt are the respective errors, A_l, A_s correspond to the relative, unnormalized amplitudes.

T / h	t_l / ns	dt_l / ns	t_s / ns	dt_s / ns	A_l	A_s
1	122	11	7	2	0.25	0.11
2	103	10	12	4	0.26	0.09
3	124	16	14	3	0.24	0.12
4	99	12	15	6	0.25	0.08

(2) Triplet kinetics

The $g^{(2)}$ function, which is obtained in the experiment, is dependent on each process that leads to fluorescence fluctuations, that is diffusion, photobleaching, singlet-triplet transitions and antibunching.[1,2] If these processes occur on timescales, which are different enough, the respective contributions can be segregated: The process of interest, in this case the antibunching decay, can then be treated separately.[3–6] Diffusional time constants of single molecules in solvents with viscosities around 1 mPa·s usually lie in the order of 100 µs, the photobleaching occurs on a much longer time scale, if at all.[7]

To prove the separation of the triplet and the antibunching time scales, we determine the intersystem crossing rate constant (isc, k_{isc}) and the rate constant for the depopulation of the triplet state, k_{risc} in two experiments in dmso. In the first one, the deprotonated form is excited with 546 nm and the intensity is varied (Fig. S2, left). 10 µM of $CsCO_3$ is added as base to ensure that no other species than the FSIP is excited. The intensity independent isc-rate k_{isc} constant is determined with equation S1, where k_{isc}^{eff} is the isc rate constant at a given excitation rate. In the second experiment, the ROH is excited with 445 nm and k_{isc} is determined in a similar manner (Fig. S2, right). Here, the proton concentration is varied instead of k_{exc}.

$$k_{isc}^{eff} = \frac{k_{isc}k_{exc}}{k_f + k_{exc}} \tag{S1}$$

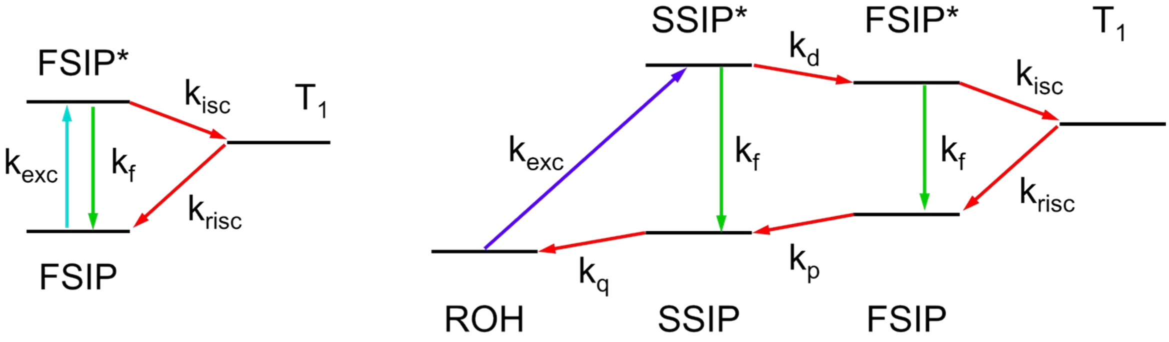

Fig. S2: Excitation schemes for the investigation of the triplet kinetics. Left: the deprotonated form is excited with 546 nm. Right: In the “Förster-cycle” experiment the ROH form is excited with 445 nm.

Tab. 2: Triplet kinetics of the photoacids used in this study in dmso. The second column lists the intensity independent rate constants for intersystem crossing. The third one provides the effective isc rate constants at 30 MHz excitation rate, which is implemented in the antibunching experiment. Together with the rate constant for bunching time constant t_B, k_{risc}, the triplet lifetime at k_{exc} = 30 MHz is obtained (fifth column).

		at k_{exc} = 30 MHz		at k_{exc} = 30 MHz
Photoacid	k_{isc} / MHz	k_{isc}^{eff} / MHz	k_{risc} / MHz	t_B / µs
(**1**)	0.98 ± 0.03	0.13 ± 0.01	0.63 ± 0.07	1.5
(**2**)	1.15 ± 0.04	0.26 ± 0.01	0.74 ± 0.03	1.3
(**3**)	0.85 ± 0.06	0.15 ± 0.02	1.41 ± 0.14	0.7

Tab. 3: The dependence of the effective inter-system crossing rate constant k_{isc}^{eff} and the bunching time t_B of the photoacid (**2**) on the proton concentration during the Förster-cycle experiment.

[msa] / mM	k_{isc}^{eff} / kHz	k_{risc} / kHz	t_B / µs
1	4 ± 3	144 ± 72	6.757
3	28 ± 7	230 ± 36	3.876
10	4 ± 1	35 ± 3	0.256
30	9 ± 1	81 ± 8	0.111
100	11 ± 1	75 ± 7	0.163

$$t_B = \frac{1}{k_{isc}^{eff} + k_{risc}} \tag{S2}$$

In the case of ROH excitation at various proton concentrations the time constant t_B (S2), on which bunching occurs, lies in the range of 6.8 µs and 0.1 µs. The corresponding antibunching decay times (the t_l component) range from ≈ 150 ns at 1 mM proton concentration to below 10 ns at > 30 mM proton concentrations.

Thus, the antibunching decay is at least 10 times faster than the triplet associated kinetics. We conclude that antibunching and triplet decay can be separately analyzed.

It is noteworthy that the time constant of the photon bunching, t_B, decreases as the proton concentration increases. We explain this unexpected bahaviour by proton quenching of the triplet state, which has been observed in the fluorescence of 2-Naphthol in a similar manner.[8]

(3) Spectral properties of (**3**)

The absorption spectra of (**3**) resemble those of compounds (**1**) and (**2**). The emission spectra of (**3**) show a stronger ROH emission than in the case of (**1**) and (**2**). The “contamination” of the analyzed photon stream by ROH photons likely explains the tendency of shorter t_s in the antibunching of compound (**3**) (see Fig. 4 a)).

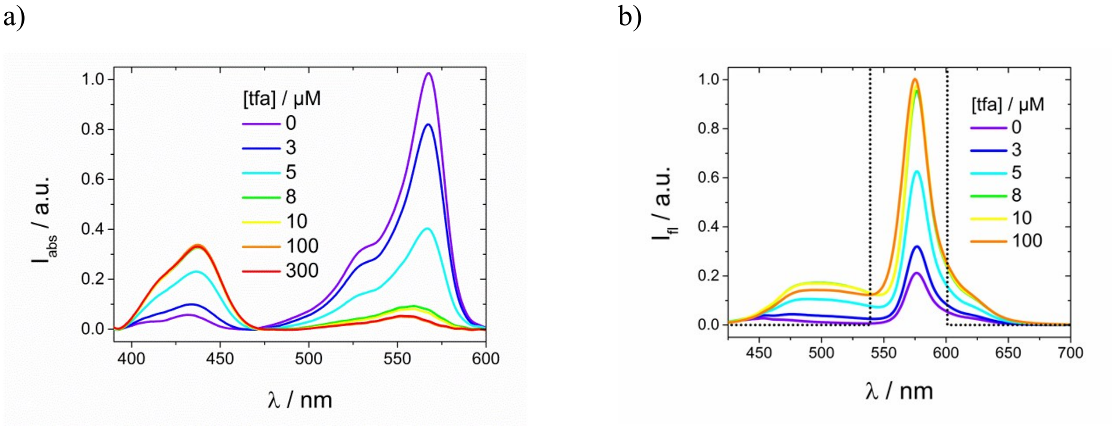

Fig. S3: Absorption a) and emission c) spectra of compound (**3**). The transmission profile of the emission filter (570/60 ET Bandpass) is also depicted in c).

(4) Experimental autocorrelation functions

Experimental correlation functions of the three photoacids (**1**)-(**3**) at 1, 2 and 3 mM tfa concentration are shown in Fig. S4 a), c) and d). The normalized fit curves are depicted in the manuscript in Fig. 3 b). Table 4 gives an overview of the associated fit parameters.

a) b)

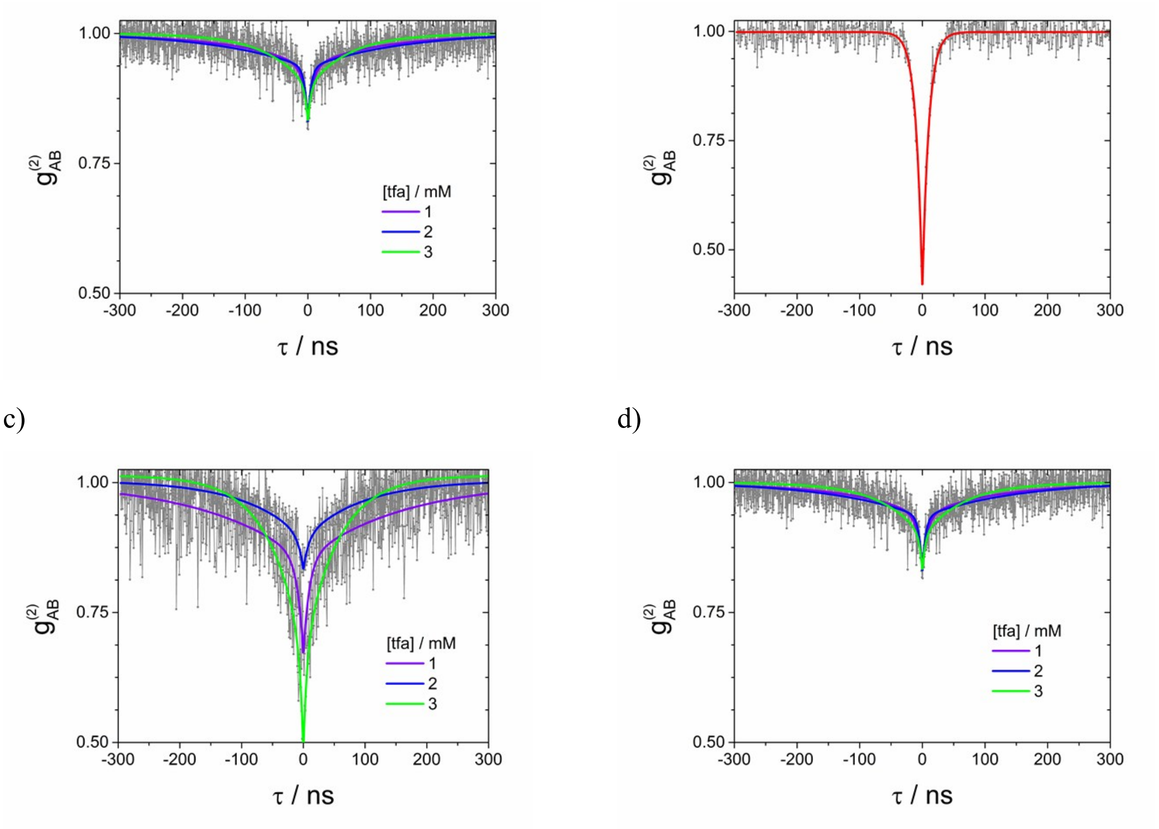

Fig. S4: Experimental correlation functions of compounds (**1**)-(**3**). a) Compound (**2**) at 1-3 mM tfa concentration. b) Compound (**2**) at 100 mM tfa. c)-d) Photoacids (**1**) and (**3**) at 1-3 mM tfa.

Tab. 4: Fit parameters of the $g_{AB}^{(2)}$ of (**1**)-(**3**) at 1-3 mM tfa concentration.

Compound	[tfa] / mM	t_l / ns	dt_l / ns	t_s / ns	dt_s / ns	A_l / %	A_s / %
(**1**)	1	161	83	9.5	3.4	46	54
	2	93	14	8.2	3.5	66	34
	3	54.4	5	5.6	2.2	66	34
(**2**)	1	156	14.2	9.3	1.3	64	36
	2	111	5.7	12.2	1.7	72	28
	3	93.8	4.7	9.3	1.8	74	26
(**3**)	1	107	35.6	8.3	2.4	40	60
	2	147	45.6	5.1	1.3	39	61
	3	64.4	10.6	4.8	2.8	61	39

(5) Antibunching decay with addition of methanesulfonic acid

To find out whether the progression of $k_l(c)$ depends on the proton donating acid or not, the antibunching measurement is repeated with methanesulfonic acid (msa) instead of trifluoroacetic acid (tfa). The influence of the proton donor on the long time component of the antibunching, respectively k_l, is negligible in the linear range, from which the bimolecular reprotonation rate constant k_p^{bi} is extracted (Fig. S5 left). Consequently, this hints to a common mechanistic reason behind the ground-state reprotonation in the linear regime. Both plots differ only in the saturation range. We ascribe this difference to slightly different dissociation of msa and tfa in dmso, which we proved by NMR spectroscopy (not shown). As a consequence, a certain acid concentration leads to a higher decay rate constant in the case of msa.

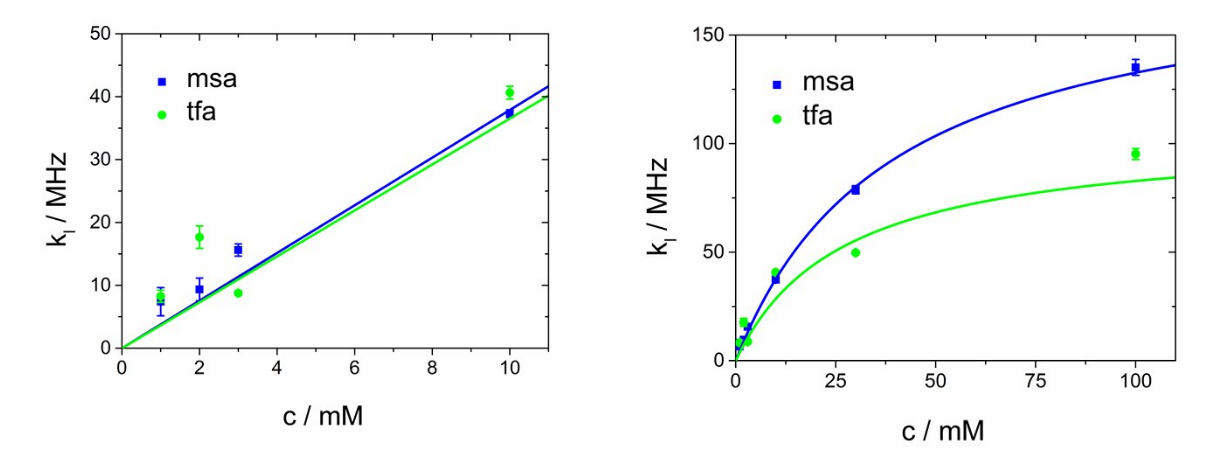

Fig. S5: Dependence of antibunching decay rate constants on proton acid concentration in the linear range and in the range of 0-100 mM.

(6) Isotope-effect

The progression of k_l(tfa) is compared to that of k_l(d-tfa) (Fig. S6), whose bimolecular rate constants differ by 5 %. This is similar to the error in the determination of the bimolecular rate constant for the different photoacids. Consequently, no clear isotope effect is detected.

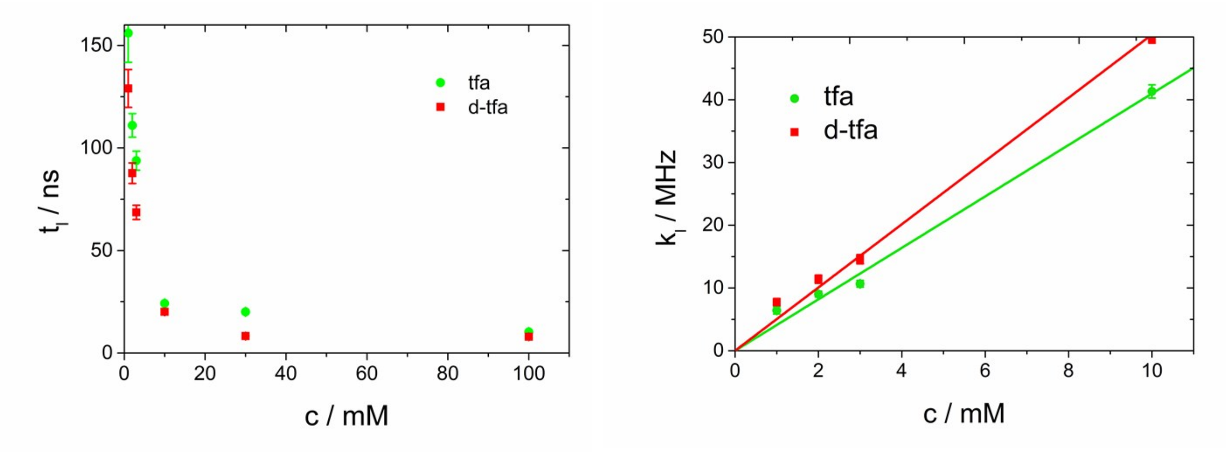

Fig. S6: Investigation of the kinetic isotope effect. The long-time decay constants (left) and decay rate constants (right) over the added amount of tfa and d-tfa, respectively. The bimolecular rate constant for protonation k_p^{bi} by tfa is 4.1 ± 0.2 x 10^9 $M^{-1}s^{-1}$ and by d-tfa 5.0 ± 0.2 x 10^9 $M^{-1}s^{-1}$.

(7) 5-states-system

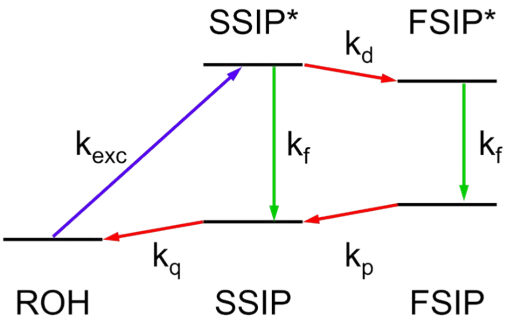

Fig. S7: 5-level-scheme.

Equation S1 collects the transitions within the 5-level-scheme.

$$\frac{d}{dt}\begin{pmatrix} FSIP^* \\ FSIP \\ ROH \\ SSIP^* \\ SSIP \end{pmatrix} = \begin{pmatrix} -k_f-s & 0 & 0 & k_d & 0 \\ k_f & -k_p-s & 0 & 0 & 0 \\ 0 & 0 & -k_{exc}-s & 0 & k_q \\ 0 & 0 & k_{exc} & -k_f-k_d-s & 0 \\ 0 & k_p & 0 & k_f & -k_q-s \end{pmatrix}\begin{pmatrix} FSIP^* \\ FSIP \\ ROH \\ SSIP^* \\ SSIP \end{pmatrix} \tag{S3}$$

or

$$\frac{d}{dt}\begin{pmatrix} FSIP^* \\ FSIP \\ ROH \\ SSIP^* \\ SSIP \end{pmatrix} = \underline{K}\begin{pmatrix} FSIP^* \\ FSIP \\ ROH \\ SSIP^* \\ SSIP \end{pmatrix} \tag{S4}$$

For the numerical calculations, $k_{exc} = 30$ MHz, $k_f = 180$ MHz, $k_d = 10$ MHz and $k_q = 330$ MHz are set and k_p is varied. S5 is chosen as initial condition as the molecule is either in the SSIP state or in the FSIP state after the emission of a photon. The distribution among FSIP and SSIP is chosen according to the amplitudes of the antibunching decays.

$$\frac{d}{dt}\begin{pmatrix} FSIP^* \\ FSIP \\ ROH \\ SSIP^* \\ SSIP \end{pmatrix}_{t=0} = \begin{pmatrix} 0 \\ 1/3 \\ 0 \\ 0 \\ 2/3 \end{pmatrix} \tag{S5}$$

(8) Dissociation constant k_d

In order to estimate the magnitude of k_d, $g_{AB}^{(2)}$ is simulated taking the 5-level scheme as basis. In the present case, k_{exc} was set to 30 MHz, k_f to 180 MHz, k_q to 330 MHz and k_p to 3 MHz. k_d is changed in the range of 3 to 30 MHz. k_f fits the fluorescence rate constant and the assumed k_p roughly matches the experimental k_p at 1 mM tfa based on a bimolecular rate constant of about 4 x 10^9 $M^{-1}s^{-1}$.

The obtained, simulated curves are compared to experimental $g_{AB}^{(2)}$ at 1 mM tfa (Fig. S8 a)). The comparison hints to experimental k_d in the range of 3 to 60 MHz. These values were initially used as input for other numerical calculations. Besides, k_d much lower than 3 MHz is not in agreement with the experiment. k_d significantly higher than 30 MHz leads to $g_{AB}^{(2)}$, which also strongly deviates from experimentally seizable correlation functions (Fig. S8 b)). We learn from suchlike simulations that k_d likely lies in the range between ≈ 1 and 60 MHz. Thus, we conclude that k_d is considerably smaller than k_f which allows us to introduce the approximation in (S9).

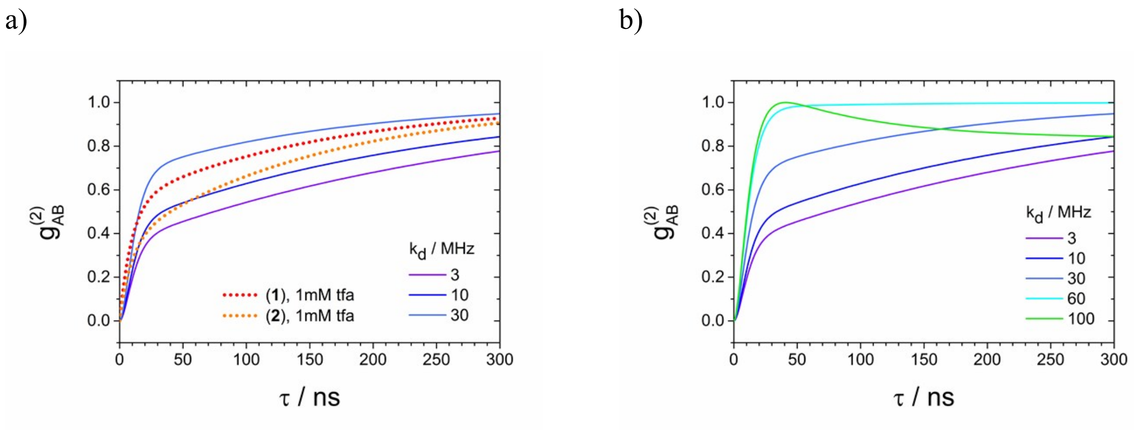

Fig. S8: a) Comparison of experimental correlation functions at 1 mM tfa and simulated data at different k_d. The simulated data is obtained by numerically solving the 5-state scheme. k_{exc} was set to 30 MHz, k_f to 180 MHz (corresponding to fluorescence lifetime), k_q to 330 MHz and k_p to 3 MHz, which roughly fits the experimental k_p at 1 mM tfa. k_d is in the range of 3 to 30 MHz at tfa concentrations between 1 to 5 mM. b) Simulated $g^{(2)}$ for k_d between 3 and 100 MHz. At k_d higher than 60 MHz, $g^{(2)}$ is no longer biexponential with two amplitudes of the same sign and, hence, do not reproduce experimental behavior.

(9) TCSPC data: Comparison of SSIP* and FSIP*

During the derivation of the $g^{(2)}$ of the five-level scheme, the SSIP* and FSIP* are assumed to decay in a similar manner. Figure S9 a) depicts the fluorescence decay of compound (**2**), which are obtained with excitation of the ROH form (405 nm) and the RO^{-} form (470 nm) respectively. In both cases, the RO^{-} fluorescence is observed. Although different excitation schemes are applied, the respective tcspc data show monoexponential decays. The associated decay constants differ by 3 % and less (Tab. 5). The apparent difference between 405 nm and 470 nm excitation in the case of (**3**) is due to the buildup of the RO^{-}* population. This buildup is less obvious is the case of (**2**) because of its distinctly higher espt rate constant. Hence, the assumption of similar decay constants of SSIP* and FSIP* is backed by the tcspc data.

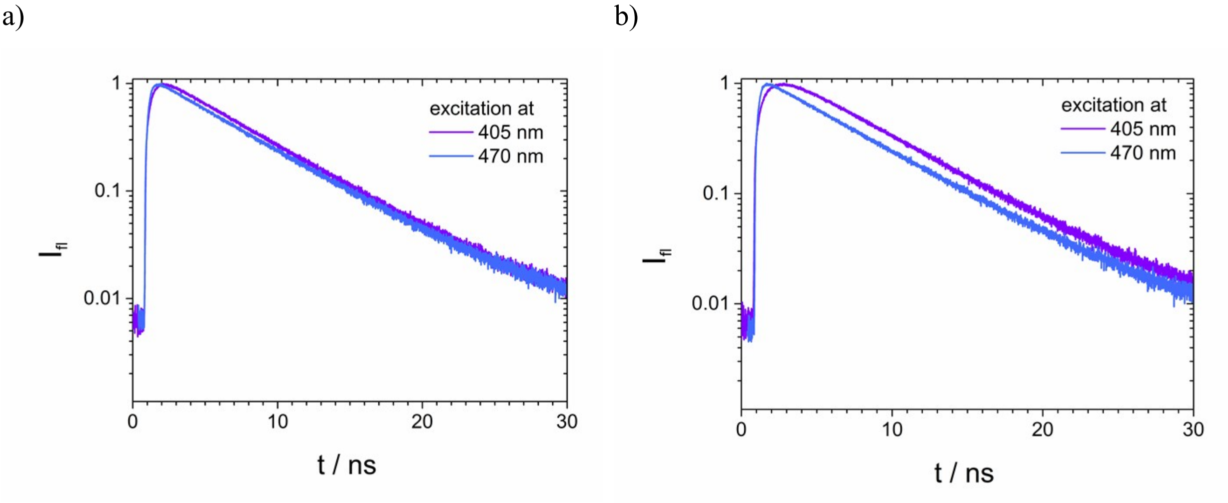

Fig. S9: Fluorescence decay of a) (**2**) and b) (**3**) in dmso with excitation at 405 nm and 470 nm. The emission filter is 570/60 ET Bandpass.

Tab. 5: Decay constants of the (**2**) and (**3**) fluorescence. The error is between 1 and 2 %.

	t / ns
(**2**), exc. at 405 nm	5.61
(**2**), exc. at 470 nm	5.78
(**3**), exc. at 405 nm	5.56
(**3**), exc. at 470 nm	5.62

(10) 3-state-system plus 2-state-system

The goal is to obtain a valid approximation of $g_{AB}^{(2)}$, which ought to be chemically interpretable. Therefore, analytical expressions for the SSIP* and the FSIP* population are obtained by splitting the five-level Eigen-Weller scheme into a 3-level-scheme and a 2-level-scheme.

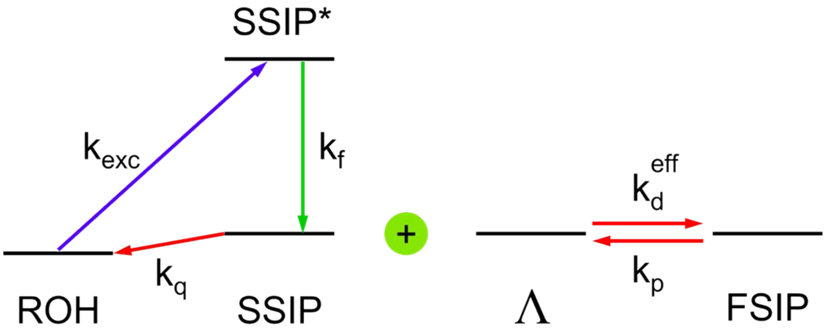

Fig. S10: Combination of 3-level and 2-level-scheme.

The transitions within the 3-level sub scheme are combined in the equations

$$\frac{d}{dt}\begin{pmatrix} ROH \\ SSIP^* \\ SSIP \end{pmatrix} = \begin{pmatrix} -k_{exc}-s & 0 & k_q \\ k_{exc} & -k_f-s & 0 \\ 0 & k_f & -k_q-s \end{pmatrix}\begin{pmatrix} ROH \\ SSIP^* \\ SSIP \end{pmatrix} \tag{S6}$$

or

$$\frac{d}{dt}\begin{pmatrix} ROH \\ SSIP^* \\ SSIP \end{pmatrix} = \underline{K_3}\begin{pmatrix} ROH \\ SSIP^* \\ SSIP \end{pmatrix} \tag{S7}$$

The molecule is found in the SSIP after the emission of a photon from the SSIP* state. Therefore, S6 is set as initial condition.

$$\frac{d}{dt}\begin{pmatrix} ROH \\ SSIP^* \\ SSIP \end{pmatrix}_{t=0} = \begin{pmatrix} 0 \\ 0 \\ 1 \end{pmatrix} \tag{S8}$$

$$det\underline{K_3} = -s\left(s^2 + s\left(k_{exc}+k_f+k_q\right) + k_{exc}k_f + k_{exc}k_q + k_fk_q\right) = -s\left(s_2 - s\right)\left(s_3 - s\right) \tag{S9}$$

with $s_1 = 0,\ s_{2,3} = -\frac{1}{2}\left(\sigma \pm \sqrt{\sigma^2 - 4\rho}\right)$ (S10)

and $\sigma = k_{exc} + k_f + k_q,\ \rho = k_{exc}k_f + k_{exc}k_q + k_fk_q$ (S11)

The implementation of the residue theorem (each pole of $\underline{K_3}$ is separated from the fraction and becomes an exponential function) leads to S12.

$$[X](t) = \sum_{i=1}^{3} \frac{det\underline{X}}{det(\underline{K_3})} exp(s_i t) \tag{S12}$$

The matrices X in S12 account for the initial conditions. So, the SSIP* matrix, which corresponds to the SSIP* state is given by S12.

$$\underline{SSIP^*} = \begin{pmatrix} -k_{exc} - s & 0 & k_q \\ k_{exc} & 0 & 0 \\ 0 & -1 & -k_q - s \end{pmatrix} \tag{S13}$$

Then, the determinant of SSIP* is

$$|\underline{SSIP^*}| =- k_{exc} k_q \tag{S14}$$

This finally leads to

$$[SSIP^*](t) = \frac{k_{exc} k_q}{s_2 s_3} + \frac{k_{exc} k_q}{s_2(s_3 - s_2)} \exp(s_2 t) + \frac{k_{exc} k_q}{s_3(s_2 - s_3)} \exp(s_3 t) \tag{S15}$$

For the 2-level-system equation S16 is valid.

$$\frac{d}{dt}\begin{pmatrix} FSIP \\ \Lambda \end{pmatrix} = \begin{pmatrix} -k_p - s & k_d^{eff} \\ k_p & -k_d^{eff} - s \end{pmatrix}\begin{pmatrix} FSIP \\ \Lambda \end{pmatrix} \tag{S16}$$

k_d^{eff} is given by (E1):

$$k_d^{eff} = k_d \frac{k_{exc}}{k_{exc} + k_f} \tag{E1}$$

In S16, Λ accounts for transitions within the three-level system.

S17 is chosen as boundary condition, because the system is in the FSIP state the moment just after the emission from the FSIP* state.

$$\frac{d}{dt}\begin{pmatrix} FSIP \\ \Lambda \end{pmatrix}_{t=0} = \begin{pmatrix} 1 \\ 0 \end{pmatrix} \tag{S17}$$

or

$$Det\underline{K_2} =- s\left(s + k_p + k_d^{eff}\right) \tag{S18}$$

with $s_4 = 0,\ s_5 =- (k_p + k_d^{eff})$ (S19)

Again, the residue theorem leads to

$$[X](t) = \sum_{i=4}^{5} \frac{det\underline{X}}{det(\underline{K_2})} exp(s_i t) \tag{S20}$$

In the present case:

$$[FSIP](t) = \frac{k_d^{eff}}{k_p + k_d^{eff}} - \frac{k_p}{k_p + k_d^{eff}} exp(-(k_p + k_d^{eff})t) \tag{S21}$$

$g^{(2)}$ is approximated by a linear combination of [SSIP*] and [FSIP].

$$g^{(2)} \propto \frac{1}{N_g}([SSIP^*] + [FSIP]) = 1 + \frac{A_2}{N_g} exp(s_2 t) + \frac{A_3}{N_g} \exp(s_3 t) - \frac{A_5}{N_g} exp(s_5 t) \tag{S22}$$

with

$$N_g = \frac{k_{exc} k_q}{s_2 s_3} + \frac{k_d^{eff}}{k_p + k_d^{eff}} \tag{S23}$$

$$A_2 = \frac{k_{exc} k_q}{s_2(s_3 - s_2)},\ A_3 = \frac{k_{exc} k_q}{s_3(s_2 - s_3)},\ A_5 = \frac{k_d^{eff}}{k_p + k_d^{eff}} \tag{S24}$$

Fig. S11 a) shows numerical solutions of the five-level Eigen-Weller scheme for various excitation rate constants k_{exc}. As input $k_f = 180$ MHz, $k_d = 10$ MHz, $k_q = 330$ MHz and $k_p = 3$ MHz is used. Thereby, k_q matches the SSIP reprotonation rate constant we determined in the antibunching experiment. In the experiment, k_d is in the range of 3 - 30 MHz (see SI 8), so k_d is set to 10 MHz for the following calculation. $k_p = 3$ MHz is expected at 1-3 mM tfa concentration. The predicted dependency of the amplitudes of the $g^{(2)}$ function (eq. S22-S24) is reflected by experimental correlation functions as depicted in Fig. S11 b).

a) b)

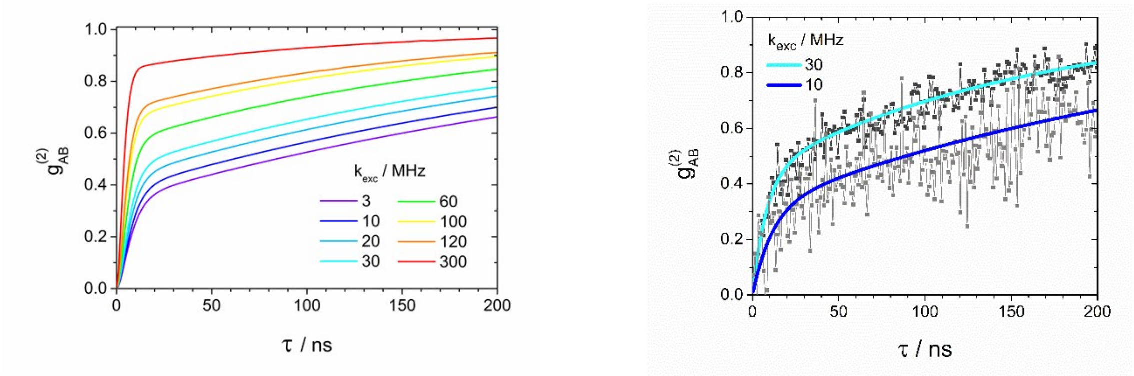

Fig. S11: a) Numerical solutions of the 5-level scheme for different k_{exc}. b) Experimental correlation functions at different excitation rate constants. These have been normalized to be comparable with the simulated curves.

In summary, k_l only changes by a factor of 2 when k_{exc} is raised from 3 MHz to 100 MHz, i.e. by a factor of about thirty (Fig. S12 a)). Based on that, the long-time component of $g_{AB}^{(2)}$ only shows a minor dependence on the applied excitation rate. The splitting of the 5-level scheme into the 3-level and the two level system is valid in a good approximation, especially at $k_{exc} \approx$ 3-100 MHz in the time range between 0 and 200 ns. The influence of k_{exc} on the relative amplitudes A_l and A_s is shown in Fig. S12 b). In the range of 0 to 300 MHz, A_l monotonically decreases as A_s increases. Also this behavior is described by our model, where A_5, which is associated with the long-time component, decreases as k_{exc}, thus also k_d^{eff}, increases. Accordingly, the 3-level-2-level approximation also describes that experimental behavior well. However, the most sensitive parameter to a variation of k_{exc} is the distribution among the amplitudes which might partially explain the experimental variation in table 4.

a) b)

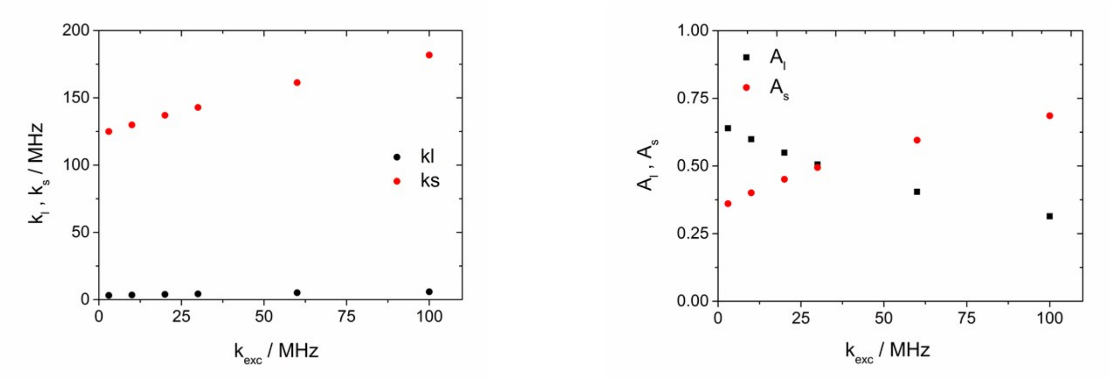

Fig. S12: a) Dependence of k_l and k_s on the excitation rate constant k_{exc}. b) Dependence of the relative amplitudes A_l and A_s on k_{exc}.

(11) Simplification of s_1 for didactic reasons

$$s_1 = {}^1\!/_2\left(-\sigma + \sqrt{\sigma^2 - 4\rho}\right) \tag{S25}$$

$$= {}^1\!/_2\left(-\sigma + \sigma\sqrt{1 - \frac{4\rho}{\sigma^2}}\right) \tag{S26}$$

$$\approx {}^1\!/_2\left(-\sigma + \sigma\left(1 - \frac{14\rho}{2\sigma^2}\right)\right) \tag{S27}$$

$$= -\frac{\rho}{\sigma} \tag{S28}$$

The approximation of the square root is assumed to be valid because of $\rho \ll \sigma$.

$$t_s \equiv -\frac{1}{s_1} \approx \frac{\sigma}{\rho} \tag{S29}$$

$$= \frac{k_q + k_{exc} + k_f}{k_q k_f + k_{exc} k_q + k_f k_{exc}} \tag{S30}$$

$$\approx \frac{k_q}{k_q k_f + k_{exc} k_q + k_f k_{exc}} + \frac{k_{exc} + k_f}{k_q k_f + k_{exc} k_q + k_f k_{exc}} \tag{S31}$$

Approximation: $k_{exc} \approx \frac{1}{6}k_f$ and $k_{exc} \approx \frac{1}{10}k_q$ thus $k_{exc} \ll k_f, k_q$

$$t_s \equiv -\frac{1}{s_1} \approx \frac{1}{k_f + k_{exc}} + \frac{1}{k_q} \tag{S32}$$

(12) TCSPC data: Geminate recombination

The fluorescence decay of the protonated form of (**2**) is shown in Fig. S13 with excitation at 405 nm, detection at 470/40 nm and with 1 mM and 1 M tfa concentration. The biexponential fit provides two time components. The short one is associated with the sum of k_f and k_{espt}, the long one with the recombination in the excited state. The diffusion-assisted geminate recombination in the excited state also explains the deviation of the decay curves from a purely biexponential behavior.[9,10] In the consequence, geminate recombination takes place within ≈ 2.5 ns. Less than 10 % of the molecules recombine in the excited state, which can be derived from the relative amplitudes A_1 and A_2. Therefore, the approximation [ROH*](t) ≈ 0 is valid in dmso with proton concentrations between 1 to 300 mM.

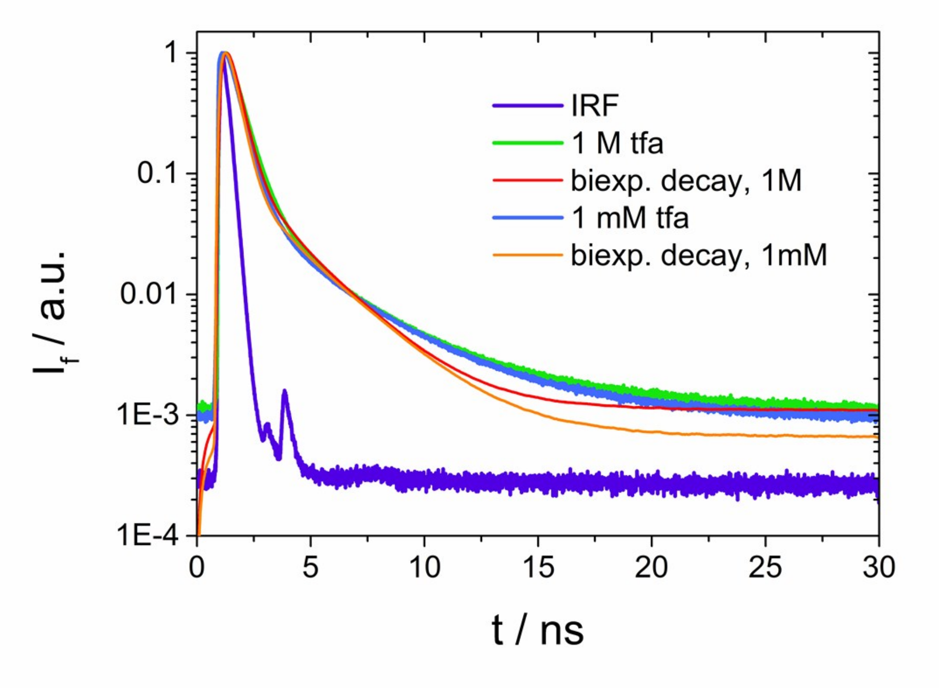

Fig. S13: Fluorescence decay of the protonated form of (**2**). Excitation at 405 nm, detection at 470/40.

Tab. 6: Parameters obtained from biexponential reconvolution fit of the tcspc data. t_1 and t_2 are the decay constants, A_1 and A_2 the respective, relative amplitudes.

	t_1 / ns	A_1	t_2 / ns	A_2
1 mM	0.401 ± 0.009	0.96 ± 0.02	2.58 ± 0.06	0.04 ± 0.01
1 M	0.468 ± 0.011	0.95 ± 0.01	2.49 ± 0.07	0.05 ± 0.01

(13) Literature

1 M. Gösch and R. Rigler, *Adv. Drug Deliv. Rev.*, 2005, **57**, 169–190.

2 O. Krichevsky and G. Bonnet, *Rep. Prog. Phys.*, 2002, **65**, 251–297.

3 I. V. Gopich and A. Szabo, *J. Chem. Phys.*, 2006, **124**, 154712.

4 D. Nettels, I. V. Gopich, A. Hoffmann and B. Schuler, *Proc. Natl. Acad. Sci. USA*, 2007, **104**, 2655–2660.

5 D. Nettels and B. Schuler, *IEEE J. Sel. Top. Quantum Electron.*, 2007, **13**, 990–995.

6 I. V. Gopich, D. Nettels, B. Schuler and A. Szabo, *J. Chem. Phys.*, 2009, **131**, 095102.

7 B. Finkler, C. Spies, M. Vester, F. Walte, K. Omlor, I. Riemann, M. Zimmer, F. Stracke, M. Gerhards and G. Jung, *Photochem. Photobiol. Sci.*, 2014, **13**, 548–562.

8 C. M. Harris and B. K. Selinger, *J. Phys. Chem.*, 1980, **84**, 891–898.

9 E. Pines, D. Huppert and N. Agmon, *J. Chem. Phys.*, 1988, **88**, 5620–5630.

10 N. Agmon, E. Pines and D. Huppert, *J. Chem. Phys.*, 1988, **88**, 5631–5638.